13B.5 Turbulence vertical structure of the boundary layer during the late afternoon transition

Clara Darbieu*(1), F. Lohou(1), M. Lothon(1), J. Vila Guerau de Arellano(2), F. Couvreux(3), P. Durand(1), D. Pino(4,5),E. G. Patton(6), E. Nilsson(1,7), E. BLay-Carreras(4).

(1) Laboratoire d'Aérologie, Toulouse, CNRS UMR 5560, University of Toulouse, Toulouse, France (2) Meteorology and Air Quality Section, Wageningen University, Wageningen, The Netherlands (3) CNRM-GAME (M étéo-France and CNRS), Toulouse, France (4) Department of Applied Physics, Universitat Politècnica de Catalunya. Barcelonatech, Barcelona, Spain (5) Institute of Space Studies of Catalonia (IEEC-UPC), Barcelona, Spain (6) National Center for Atmospheric Research, Boulder, Colorado, USA (7) Uppsala University, Uppsala, Sweden

1. Introduction

The transition from a well-mixed convective boundary layer to a residual layer overlying a stabilized nocturnal layer raises several issues, which remain difficult to address from both modeling and observational perspectives. The well mixed convective boundary layer with fully developed turbulence is mainly forced by buoyancy. The daily decrease of the surface buoyancy flux leads to the decay of the turbulence kinetic energy (TKE), and a possible change of the structure of the turbulence before it reaches the stable regime, which shows more anisotropy and intermittency. It is important to better understand these processes, as it can impact on the dispersion of tracers in the atmosphere, and on the development of the nocturnal and daytime boundary layers of the following days (Blay-Carreras et al., 2014).

The turbulence decay has been studied with laboratory experiments (Monin and Yaglom (1975), Cole and Fernando (1998)), numerical studies with Large Eddy Simulations (LES) (Nieuwstadt and Brost (1986), Sorbjan (1997)) and observations (Fitzarrald et al 2004, Grant 1997). In all of them, the decay is mainly related to the decrease of the surface buoyancy flux, but with complexity gained with shear-driven boundary layers (Pino et al. (2006), Goulart et al. (2003)), which slow the decay. Nieuwstadt and Brost (1986) considered a sudden shut off of driving heat flux, and found that the decay occurred at a period of the order of $t_* = z_i/w_*$, where z_i is the planetary boundary layer (PBL) depth, and w_* is the convective velocity scale (Deardorff, 1970). It is very different to consider a slower decrease of the forcing surface buoyancy flux, which would have a time scale of τ_f (Sorbjan (1997), Rizza et al. (2013), Nadeau et al. (2011)). If τ_f is large relative to t_*, the turbulence can adjust to the forcing change, in quasi-equilibrium, as noted by Cole and Fernando (1998). This is the case in the mid-afternoon PBL, when t_* is around 10 or 15 min and τ_f is around 2 or 3h. Sorbjan (1997) found that the turbulence kinetic energy decay was scaling with τ_f/t_*, with t_* estimate at the start of the decay. But in late afternoon and sunset, t_* starts to increase significantly (until the definition of w_* is put into question at zero buoyancy flux), and turbulence may not be able to adjust to the external change. More description of the turbulence structure is needed to better understand this decay process in the PBL.

The evolution of the turbulence lengthscales has not been addressed extensively, but several studies can be found which do not necessarily converge. With fundamental consideration of eddy life-time, or turn over time scale, one may state that smaller eddies will decay earlier than larger eddies (Davidson, 2004). This is one explanation given by Sorbjan (1997) for the increase of the characteristic lengthscale of the vertical velocity found in the mixed (then residual) layer of the LES. To the contrary, with tethered-balloon observations, Grant (1997) showed that the peak of the vertical velocity spectra shifts to smaller length scales during the evening transition. Finally, Nieuwstadt and Brost (1986) and Pino et al. (2006) found that the length scale of maximum spectral energy of the vertical velocity remained constant during the decay process. Pino et al. (2006) also have shown that the characteristic length scales increase with time for all other meteorological variables: the horizontal wind components and the temperature and moisture scalars.

The evolution of the turbulence scales remains unclear and only partly understood. It must be thoroughly investigated whether the scales in the mixed and afterward residual layer really increase or not. Considering the time response and equilibrium aspect mentioned above, and the possible decoupling with height between the stabilizing surface layer and the overlying residual layer, it is also important to consider the vertical structure of the turbulence decay, that is the evolution of turbulence and scales as a function of height. In the surface layer, one may expect the lengthscales to decrease, as infered from the study by Kaimal et al. (1972) of the evolution of spectra with stability observed at surface based on the Kansas experiment.

*corresponding author address: Clara Darbieu, Centre de Recherches Atmosphériques, 8 route de Lannemezan, 65300 Campistrous, France; *email*: clara.darbieu@aero.obs-mip.fr

The numerical studies often considered the TKE decay integrated over the entire PBL depth, and observations of the turbulence decay were made most of the time at surface, but only few observational studies considered the vertical structure of the TKE decay (Grant (1997) in stable layer, Fitzjarrald et al. (2004) in afternoon decaying PBL).

Here we investigate the evolution of the turbulence spectra and scales during the afternoon transition based on the BLLAST (Boundary Layer Late Afternoon and Sunset Turbulence) dataset, collected during summer 2011. A well-documented cloud-free weak wind day is considered here to analyze in details the evolution of the turbulence along the day, from midday to sunset, with both observations and a Large Eddy Simulation (LES). Our analysis aims at (1) testing the capability of the LES to represent the turbulence structure of the afternoon decay, (2) evaluating the evolution of integral scales, turbulence kinetic energy, shape of the spectra in both observations and numerical simulation, and as a function of height, (3) understanding the potential decoupling with height that may occur during the afternoon and evening transitions.

After a presentation of the experimental dataset and the LES configuration (§2.), the case study of the 20th of June is described through the observations, the LES initialisation and evaluation (section 3.). The working assumptions and methods used in this study are then detailed (section 4.) before presenting and discussing the results (section 5.). Concluding remarks are given in section 6..

2. Experimental dataset and LES configuration

The BLLAST experiment provides a large dataset to investigate the vertical structure of the decaying PBL. A detailed description of the experiment, instrumentation and data processing are provided in Lothon et al. (2014). As a complementary tool, a LES of an ideal case is initialized with the BLLAST observations to study turbulence decay over an homogeneous and flat surface. The simulated turbulence structure is compared to the observations, and aims at testing the LES capacities during this challenging period, and studying more finely the vertical and temporal evolution of the turbulence in the PBL.

2.1 Experimental dataset

In this study, we use radiosoundings, aircraft and surface measurements. Figure 1 represents the normalized altitude z/z_i of the stagged legs flown by the aircraft as well as the different launching times of the radiosoundings (the method used for z_i estimation is discussed later). In order to monitor the evolution of the mean structure of the PBL during the LAT (and initialize the simulation), we use standard radiosoundings launched every 6 hours, from 0600 UTC to 1800 UTC, and hourly radiosoundings (Legain et al., 2013) of the low troposphere (up to 3 to 4 km height), from 1300 to 1800 UTC. The launching sites of the two types of radiosoundings are 4 km apart. The radiosoundings measured the temperature, the water vapour content and the sonde location from which the horizontal wind components are deduced.

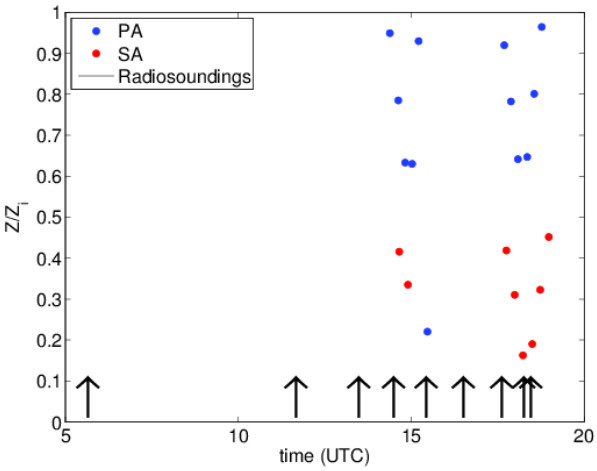

Figure 1: normalized altitude z/z_i (where z_i is the boundary layer height) of the legs flown by the two aircraft the 20 june 2011 (piper aztec in blue, sky arrow in red) and launching times of the radiosoundings (black arrows).

Surface energy balance and turbulence structure in the surface layer are provided by several ground stations implemented over different vegetation coverages (wheat, moor, corn, grass, forest and prairies). A permanent 60 m tower, equipped at 30 m, 45 m and 60 m provides a vertical profile of turbulence in the surface layer. The statistical moments are estimated over 30-minute sample with 10 Hz frequency measurements. The surface heat fluxes are used as surface forcing in the simulation.

Two aircraft, the French Piper Aztec (PA) from SAFIRE (Saïd et al., 2005) and the Italian Sky Arrow (SA) from Ibimet and Isafom (Gioli et al., 2009), flew extensively during the afternoon, respectively at 65 $m\,s^{-1}$ and 40 $m\,s^{-1}$. They measured temperature, moisture, pressure, CO_2 concentration and 3-D wind at respectively 50 Hz (SA) and 25 Hz (PA) along 25 to 40 km long legs stabilized in attitude and altitude. The detailed instrumentation of both aircraft is given in Lothon et al. (2014).

Depending on the meteorological situation and the scientific interest, different flight patterns were performed: PA and SA flew either simultaneously in order to have a

better spatial coverage, or one after the other to have a better time coverage. For the selected case study, the two aircraft flew simultaneously, the SA flying above the PA. As shown in Fig. 1, they flew along three parallel legs, at three latitudes and at six heights within the BL, and two different time periods: the first one from 1430 UTC to 1530 UTC, the second one later, from 1745 UTC to 1900 UTC. This flight strategy gives access to six heights to study the vertical structure of the turbulence within the PBL.

2.2 LES configuration

The LES code from NCAR (Moeng (1984), Sullivan and Patton (2011), Patton et al. (2005)) is based on Navier-Stokes equations, including conservation laws for momentum, mass and the first law of thermodynamics. An idealized simulation is initialized with early morning radiosoundings and forced with observed surface heat flux and prescribed advection.

The simulation resolves a domain of $10.24 \times 10.24\, km^2$ horizontally and 3.072 km vertically, with $\Delta_x = \Delta_y = 40\, m$ and $\Delta_z = 12\, m$ of horizontal and vertical resolution, respectively. This results from a compromise bewteen the computation time and three constraints: 1/ the domain size and resolution were chosen after a sensitivity study (not shown) so that the modeled spectra were covering correctly the wavenumber ranges in order to be able to represent the characteristics of the observed spectra, 2/ the resolution was chosen so that the ratio of z_i to $(\Delta_x \times \Delta_y \times \Delta_z)^{1/3}$ was large enough to ensure that the results are independent of the resolution (Sullivan and Patton, 2011), and, 3/ the ratio of Δ_x to Δ_z be kept small, but a high enough vertical resolution is needed to correctly represent the entrainment zone (Sullivan and Patton, 2011). The time step evolves during the simulation and is about 1.4 s for fully convective conditions.

The braket notation $\langle \psi \rangle$ for any simulated variable ψ is used to represent the 2D-horizontal average. The same notation is used for the 1D-horizontal average of the airborne measurements along the legs. For the surface dataset, $\bar{\psi}$ represents the time average notation. For these three types of datasets, the turbulent fluctuations ψ' are defined as deviations from the corresponding mean. For a better comparison with simulated variances, variances from measurements are estimated by integration of the observed spectra over the wavenumber range resolved in the simulation. At last, all the simulated mean vertical profiles presented herefater are averaged over 30 minutes and noted for simplicity with the braket notation $\langle \psi \rangle$, which then indicates both horizontal and temporal average.

3. Case study

3.1 case description

The 20 June 2011 was selected as the case study on the basis of meteorological criteria and data coverage. The synoptic situation was a high pressure system over South-West of France, with a light westerly wind leading to a fair and cloud-free weather.

Figure 2 represents the evolution of the radiosoundings of the potential temperature θ and the wind direction from 0500 to 1800 UTC on 20 June 2011. During the day, the PBL warms up of about 10 K and the boundary layer height z_i, defined as the height of the maximum of relative humidity, grows up to about 1100 m. Figure 2a also shows some warm advection above the PBL between 0515 UTC and 1100 UTC, that needs to be taken into account in the simulation. After 1100 UTC, the lapse rate of θ hardly changes, meaning that the temperature advection likely becomes very weak. Figure 2b shows that there is an easterly wind within the PBL, veering to Westerly above. The wind is weak within the PBL (less than 4 $m\, s^{-1}$) and increases with height, up to 10 $m\, s^{-1}$ at 1500 m. It remains constant all along the day. The water vapour mixing ratio increases from 8 to 10 $g\, kg^{-1}$ in the PBL until 1300 UTC and decreases afterward. The temporal evolution of the PBL mean vertical structure is further analysed in section 3.3.

The surface sensible and latent heat fluxes (H and LE, respectively) measured above various vegetation coverages are presented in Fig. 3. The maximum value of H varies from 130 $W\, m^{-2}$ over grass and moor and 350 $W\, m^{-2}$ over the pine forest. LE shows much less variability between vegetation coverages, varying from 250 $W\, m^{-2}$ to 350 $W\, m^{-2}$. The measurements at 60 m height integrate a large footprint and should give flux estimates of the heterogeneous landscape. This is the case for the 60-m height estimate of H whose daily variation is encompassed in all the others and close to the moor and grass, the most represented vegetation covers over the plateau.

In this study, the afternoon transition is defined as the period from the time when the buoyancy flux is maximum, to the time where it goes to zero. This period varies according to the surface (Lothon et al., 2014). For the moor coverage, which will be used as surface boundary in the simulation of the 20 June 2011, this period starts at 1200 UTC and ends at 1750 UTC, while it ends 20 minutes earlier when considering H instead of the buoyancy flux. This delay is observed for all the IOP days of the BLLAST campaign implying that the latent heat flux reaches zero systematically later than the sensible heat flux. Thus the forcing time scale of the flux decay τ_f is around 5.8 hours for the moor site and therefore in the simulation.

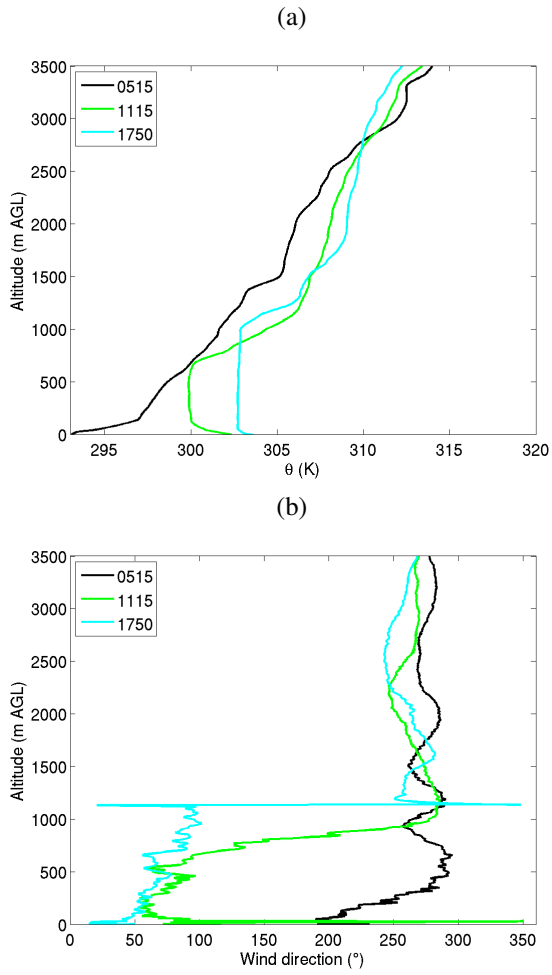

Figure 2: radiosoundings of (a) the potential temperature θ and (b) the wind direction on the 20 june 2011.

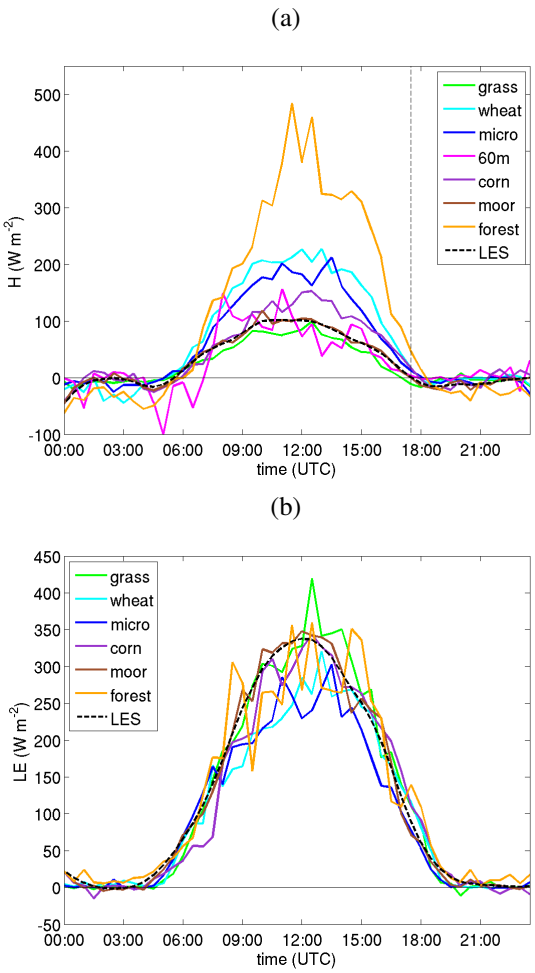

Figure 3: temporal evolution of (a) surface sensible (h) and (b) latent (le) heat fluxes over several vegetation coverage, on the 20 june 2011. the vertical dashed lines stand for the maximum surface bouyancy flux (at 1200 utc) and its zero value (at 1745 utc).

3.2 LES initialization

The simulation was initialized early in the morning, in order to ensure a well built turbulence in the convective PBL by the afternoon. The simplified wind, temperature and humidity initial profiles were deduced from the 0515 UTC radiosounding and are represented in Fig. 4. An homogenous surface is considered in the LES with imposed surface fluxes which are those measured at the moor site (Fig. 3).

The estimate of the advection was made using AROME forecast model and reveals predominant zonal advection, especially during the morning. Temperature and humidity vertical profiles of total advection (horizontal advection plus subsidence) are imposed in the simulation every one hour, based on AROME forecast model. The total advection was estimated on 16 grid points in a box surrounding the experimental site, the spatial resolution being 2.5 km in AROME. The total advection profiles from AROME were smoothed in time, and imposed to decrease exponentially above 2500 m for temperature and humidity. Below 600 m, advection of temperature was also imposed to decrease exponentially toward zero since the AROME temperature advection was overestimated compared to observations.

From 0515 UTC to 1000 UTC, the temperature advection is important and about 10 $K\ day^{-1}$ from 500 m up to 1500 m (not shown). After 1100 UTC, it decreases and is negligible in the afternoon. This is consistent with what is observed on the evolution of the potential temperature (Fig. 2a). From morning to 1400 UTC, the moisture advection is about -10 $g\ kg^{-1}\ day^{-1}$ from surface up to 500 m, and about 10 $g\ kg^{-1}\ day^{-1}$ above. After 1400 UTC,

the moisture advection is much weaker (not shown).

The data files used to run this case (initial profiles, surface flux and advection profiles) are available on the website of the BLLAST database (http://bllast.sedoo.fr/database).

3.3 Evaluation of the simulated boundary layer

The evolution of θ vertical profiles in the simulation is compared with radiosoundings in Fig. 4a. The simulated θ is close to the observations with a good evolution of θ in the mixed layer and a well simulated lapse rate decrease between 0515 UTC and 1115 UTC due to the prescribed advection. Figure 4b presents the evolution of the water vapour mixing ratio r. The temporal evolution of r profiles shows a well simulated daily humidification though the complex vertical variability of the profiles is not reproduced. One can notice a 1 $g\ kg^{-1}$ drier mixed layer at 1300 and 1800 UTC than actually observed.

The horizontal mean wind speed is well reproduced in the simulation during the day: the wind remains weak (about 3 $m\ s^{-1}$ below 1000 m, see Fig. 4c), and increases with altitude to reach 10 $m\ s^{-1}$ at 2000 m. No wind forcing is prescribed in the simulation, therefore the observed wind direction change from West to East within the mixed layer between 0500 and 1100 UTC is not simulated (Fig. 4d). Whilst the wind speed shear is well simulated, the wind direction shear is underestimated and consequently the entrainement processes (Pino et al., 2006) might not be as important in the simulation as in reality.

The vertical profiles of the buoyancy flux (Fig. 5) have a quite classical shape until 1330 UTC with a linear decrease with height and negative flux above 0.8 z_i. After 1330 UTC, the upper layer characterized by negative entrainment flux deepens and goes down to 0.4 z_i at 1730 UTC. During the afternoon transition the entrainment ratio (minus buoyancy flux at the top of the PBL to the buoyancy flux at surface) remains constant and about 0.13 (not show). Unfortunatly, this value can not be compared to observations since the fluxes deduced from airborne measurements in the PBL vary a lot at that time, and because of lack of statistics of the large scales in a less and less stationnary PBL.

The temporal evolution of z_i has been estimated from UHF and radiosoundings measurements and compared to z_i in the simulation (Fig. 6). From UHF, z_i is estimated as the maximum of the refractive structure coefficient (Heo et al. (2003), Jacoby-Koaly et al. (2002)). From radiosoundings, z_i is estimated as the altitude of the maximum relative humidity below 2500 m. In the simulation, z_i is estimated as the height of the mixed layer, determined with a threshold on the θ vertical gradient slope. This method was prefered to the one used for radiosoundings because of the complex humidity profiles which lead

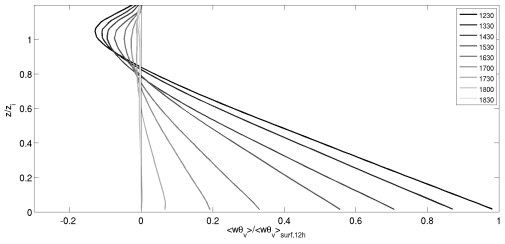

Figure 5: temporal evolution of the resolved tke at different heights (different colors), with les (continuous lines), aircraft and surface measurements (open and filled circles, respectively). the vertical dashed lines stand for the maximum surface bouyancy flux (at 1200 utc) and its zero value (at 1745 utc).

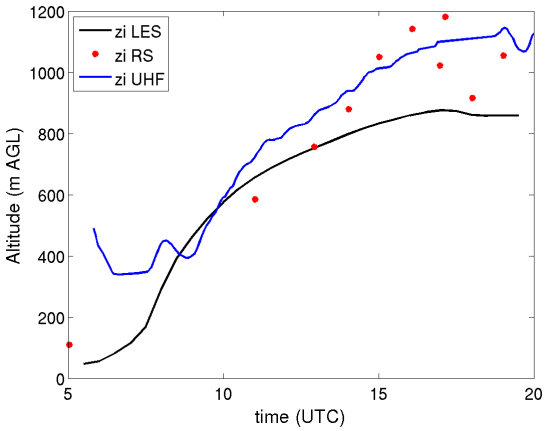

Figure 6: temporal evolution of the boundary layer height z_i, (black line) in the simulation, from (red dots) radiosoundings and (blue line) uhf.

to more fluctuating z_i estimates. However, the difference between these two estimates is less than 50 m.

Until 0900 UTC, the UHF detects the residual layer of the previous day. After 1000 UTC, z_i increase is similarly depicted by the UHF and radiosoundings. The simulated PBL follows quite well the estimations of z_i from the observations until 1300 UTC and develops up to 850 m. Then z_i remains constant in the simulation whereas, according to radiosoundings and UHF, z_i increases up to 1100 m. This discrepancy between observed and simulated z_i in the afternoon might be partly explained by a weaker entrainement effect in the simulation due to a lack of wind shear.

The temporal evolution of the resolved and observed TKE at several heights is presented in Fig. 7. For a better comparison, the variances estimated from measure-

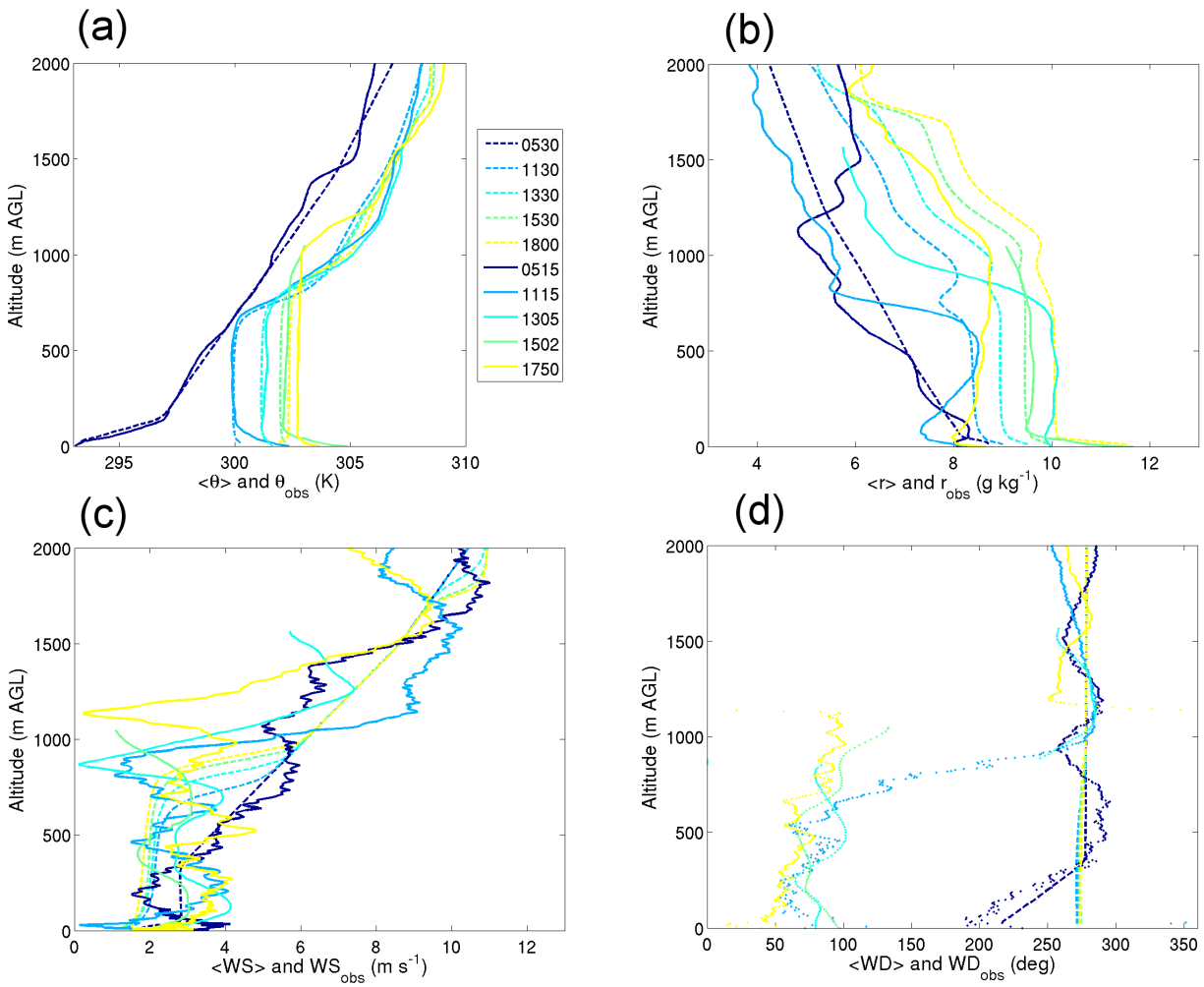

Figure 4: evolution of (dashed lines) the simulated and (continuous lines) observed vertical profiles of (a) potential temperature θ ,(b) mixing ratio r ,(c) wind speed (ws), (d) wind direction (wd).

ments are obtained from the integration of the spectra over the wavenumber range of the simulation. The LES underestimates the TKE with a factor 2 compared to the observations.

One must keep in mind that we did not aim at reproducing exactly the observed PBL but at simulating an ideal case whose set up is partly constrained by the BLLAST data. The mean evolution of the PBL is still quite well represented but with some noticeable differences: a lower development of the PBL of about 200 m, an underestimated TKE with a factor of 2 and a wind shear in direction not reproduced. Despite these differences on the main PBL structure, the observed and simulated turbulence characteristics along the afternoon will be compared and analysed. The next section presents the methods used to deduce the turbulence characteristics from the spectra.

4. working assumptions and methods

A broad overview of the turbulent conditions during the afternoon is depicted through the analysis of the TKE temporal evolution at different heights in the PBL, the TKE reading

$$TKE = \frac{1}{2}(\sigma_u^2 + \sigma_v^2 + \sigma_w^2), \qquad (1)$$

where σ_u^2, σ_v^2 and σ_w^2 are the variances of the horizontal wind components u, v, and the vertical wind component w.

The energy distribution among the different eddy scales is then studied through a spectral analysis of the vertical air velocity w within the entire PBL. The evolution of w spectra characteristics is analyzed by the use of an analytical spectra model.

This study focuses on w because simulated and ob-

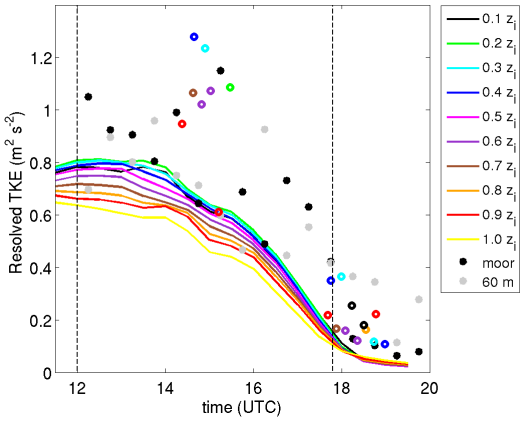

Figure 7: temporal evolution of the resolved tke at different heights (different colors), with les (continuous lines), aircraft and surface measurements (open and filled circles, respectively). the vertical dashed lines stand for the maximum surface bouyancy flux (at 1200 utc) and its zero value (at 1745 utc).

served w spectra are more easily comparable than the spectra of the horizontal components. Indeed, the horizontal components have usually significant energy at low wavenumber in the observations which can not be represented in the simulation due to the limited simulated domain. Therefore, working on w spectra is a first step investigated in this study which should be completed with the horizontal components and scalars studies later on.

The choice of the analytical spectra is now discussed since several models exist for convective conditions. Among others, the Kaimal et al. (1976) spectral model is well known for surface and mixed layer and was validated with Kansas surface layer measurements and with Minnesota measurements in the mixed layer. The von Kàrmàn spectral model (Kàrmàn, 1948) is also widely used for isotropic turbulence. Hojstrup (1982) proposed a more generalized model for w spectra up to $z/z_i = 0.5$, based on a function of stability from neutral to very unstable. However many of these analytical models were validated for unstable near surface conditions and a few of them are able to adapt within the entire convective PBL (Lothon et al., 2009). Among several analytical models tested, the general kinematic spectral model for anisotropic horizontally homogeneous turbulent field from Kristensen and Lenschow (1989) is the one which better fits the observed spectra at surface and in the boundary layer acquired during the BLLAST field campaign. For w, the model writes:

$$\frac{S_{Kris}(k)}{\sigma_w^2} = co\frac{l_w}{2\pi}\frac{1+\frac{8}{3}(\frac{l_w k}{a(\mu)})^{2\mu}}{(1+(\frac{l_w k}{a(\mu)})^{2\mu})^{5/(6\mu)+1}}, \qquad (2)$$

where

$$a(\mu) = \pi\frac{\mu\Gamma(\frac{5}{6\mu})}{\Gamma(\frac{1}{2\mu})\Gamma(\frac{1}{3\mu})}, \qquad (3)$$

k being the wavenumber along the trajectory of the airplane, or along the x axis in the simulation, and in the mean wind direction for surface measurements. Γ is the gamma function. co is a coefficient which ajusts the

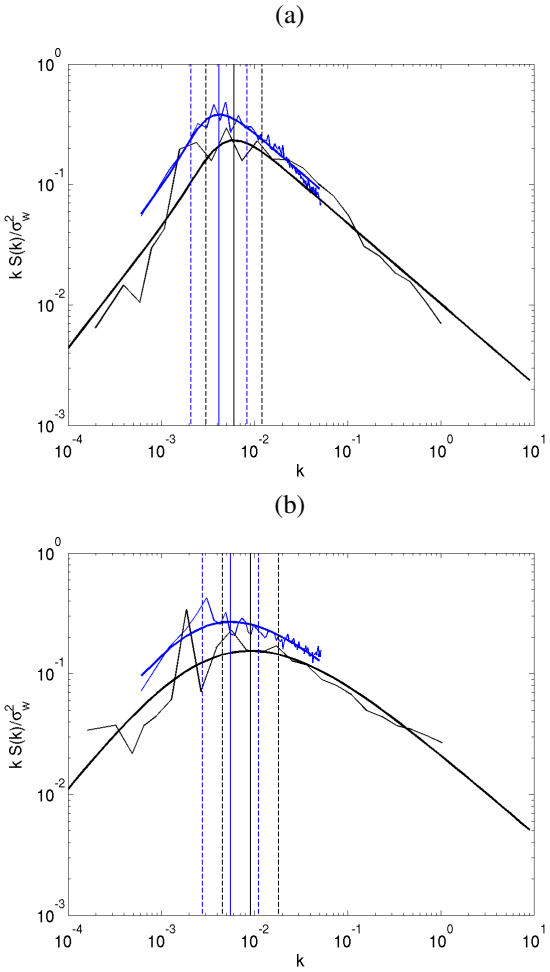

Figure 8: example of two normalized w spectra at (a) 1500 and (b) 1800 utc from both aircraft (black) and les (blue), fitted with the kristensen analytical spectral model (thick lines). the vertical continous lines represent λ_w, the maximum energy wavenumber and the dashed vertical lines represent k_1 and k_2, the limits of the low wavenumber range and of the inertial subrange, defined as $k_1 = \pi/\lambda_w$ and $k_2 = 4\pi/\lambda_w$.

amount of energy because σ_w^2 is calculated over a finite domain of wavenumbers instead of over the theoretically infinite domain. This model has two others characteristic parameters: the integral lengthscale l_w, which is a characteristic scale corresponding to the scales over which w remains correlated with itself (Lenschow and Stankov, 1986), and a sharpness parameter μ, which governs the curvature of the spectra in the region of the peak, between the low wavenumber range and the inertial subrange. The larger μ, the sharper the peak. According to equation (2), the Kristensen and Lenschow (1989) model gives the Kaimal et al. (1972) spectrum for $\mu = 0.5$ and the Kàrmàn (1948) spectrum for $\mu = 1$. It is thus a more generalized model, able to adapt to a larger range of conditions. Note that l_w is related to the wavelength of the density energy maximum (Λ_w) by a monotonic function of μ:

$$\Lambda_w = \left\{ \frac{5}{3}\sqrt{\mu^2 + \frac{6}{5}\mu + 1} - (\frac{5}{3}\mu + 1) \right\}^{\frac{1}{2\mu}} \frac{2\pi}{a(\mu)} l_w. \quad (4)$$

The model is fitted to each observed and simulated spectrum, by finding the best [co, l_w, μ] triplet using a logarithmic least squares difference method.

Note that the integral scales of w is classically calculated from w autocovariance function R_w, since it is defined as (Lenschow and Stankov, 1986):

$$L_w = \int_0^\infty R_w(r) dr, \quad (5)$$

r being the displacement.

In this study, L_w, obtained using an integration until the first zero of $R_w(r)$, is used as a reference for l_w deduced from the kristensen spectral fit and enables a comparison with litterature.

The spectra of w are calculated using Taylor's hypothesis of frozen turbulence. The spectra based on surface measurements are calculated over 30 minute samples, which is a good compromise between a sufficient number of eddies and stationary conditions. The spectra based on the aircraft measurements are calculated on 35 km-long legs in average. To ensure a good consistency between simulated and observed spectra, one-dimensional simulated spectra are also considered in the LES. They are calculated along the x directions and averaged along the y direction. Simulated spectra are estimated above the fourth level (to ensure a negligeable contribution of the subgrid scale) and every 96 m in the vertical. The same sampling is used to calculate the autocorrelation functions for L_w estimates.

In order to study the evolution of the spectral slopes in specific domains, the wavenumber range is split in three parts: 1/ the low wavenumber range $]0, k_1]$, 2/ the region around the maximum density energy at $k = 2\pi/\Lambda_w$, $[k_1, k_2]$, 3/ the inertial subrange $[k_2, \infty[$. The limits of the low wavenumber range and of the inertial subrange depend on the scale at maximum energy Λ_w and is defined here with $k_1 = \pi/\Lambda_w$ and $k_2 = 4\pi/\Lambda_w$.

The fit of the observed or simulated spectra by the Kristensen analytical model is an important step of the method used in this study, therefore its quality needs to be verified.

The quality index of the analytical fit is estimated based on the ratio between the observed (respectively simulated) spectrum and the analytical spectrum:

$$IQ_{obs} = \frac{1}{N_{obs}} \Sigma \left| \log \left(\frac{S_{obs}}{S_{Kris}} \right) \right|, \quad (6)$$

$$IQ_{LES} = \frac{1}{N_{LES}} \Sigma \left| \log \left(\frac{S_{LES}}{S_{Kris}} \right) \right|, \quad (7)$$

where S_{obs} is the spectrum calculated from the observed w, S_{LES} is the spectrum calculated from the simulated w, and S_{Kris} is the analytical spectrum from equation (2) that best fits the observed or simulated spectra. N is the number of wavenumber datapoints on which S is defined. The larger IQ_{obs} (IQ_{LES}), the larger the departure between the observed (simulated) and the analytical spectra.

Figure 8 presents two normalized spectra of w from both aircraft and simulated data, fitted with the Kristensen analytical spectra model. The aircraft (simulated) spectra are calculated at 1500 UTC and 1800 UTC and at $z = 0.6\ z_i$ ($z = 0.6 - 0.75\ z_i$ slice-averaged). This figure shows first the ability of the simulation to reproduce properly both the energy production domain and the inertial subrange, and second, the ability of the analytical spectra model to fit well the observed and simulated spectra in mid-afternoon convective conditions (1500 UTC) and at the end of the afternoon (1800 UTC).

For those two examples, $IQ_{obs} = 0.11$ and $IQ_{LES} = 0.02$ at 1500 UTC, and $IQ_{obs} = 0.10$ and $IQ_{LES} = 0.015$ at 1800 UTC. In general, the quality index for the observations are about 5 to 10 times larger than for the LES (not shown). This is due to the lack of statistics at large scales in observations, leading to larger fluctations in the spectral density energy for the first domain (low wavenumbers). For the aircraft observations especially, IQ_{obs} was mainly dominated by the departure from the analytical spectrum at low wavenumber. This is due to meso or submeso- scale features that cannot be well sampled along the 1D 30-km sample, but are typical of the observed boundary layer. There is no such contribution in LES simulation, so that the modeled spectra have less uncertainty at low wavenumbers.

We also found that the quality index for observed and simulated data were found to generaly remain constant until 1900 UTC, but for simulated data above 0.6 z_i, IQ_{LES} increases from 0.02 to 0.045 after 1830 UTC. This means

that the spectra fit is equally reliable throughout the afternoon transition, allowing the study of the time evolution of the spectra characteristics from the convective conditions until near neutral conditions.

The spectra changes throughout the LAT, already noticeable in Fig. 8 with Λ_w shift toward longer wavelength, the spectra flattening and the inertial subrange slope change, are further quantified and discussed in the following section.

5. results

5.1 tke decay from surface to pbl top

(a)

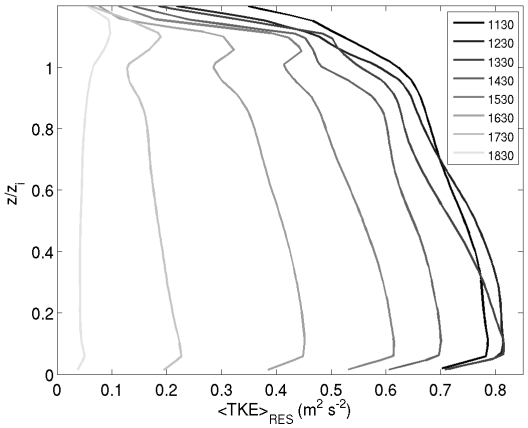

(b)

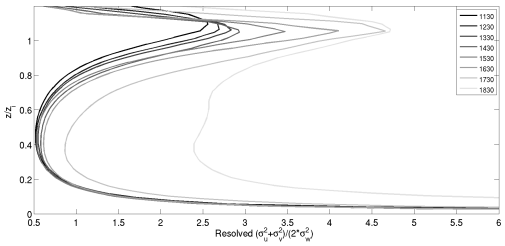

Figure 9: evolution of the vertical profiles of resolved (a) tke and (b) anisotropy.

Most of the previous studies on turbulence decay were done with either vertically integrated simulated TKE over PBL depth or measured TKE in the surface layer. The decay of turbulence up to the top of the mixed or residual layer remains little documented.

Figure Fig. 9a shows the evolution of the vertical profiles of the resolved TKE in the LES from 1130 UTC to 1830 UTC. Those 30 minutes averaged vertical profiles are presented each hour. They show that the TKE decreases over the whole depth of the CBL, but that there is a delay of one hour between the start of the decay at the top and the start at the bottom: at 1230 UTC, the TKE continues to increase in the lower CBL, while it has started to decrease in the upper part. Later on, after 1530 UTC, the decay is homogeneous over the vertical.

It is interesting to see that the TKE subtly starts to decay from the top in the LES, hereafter called a top-down decay. This, unfortunately, is too subtil (and also too early) to be seen from the aircraft observations. However, observations of TKE dissipation rates by UHF wind profiler that day also show a top-down decay of the dissipation rate that starts around 1330 UTC (not shown). It is also consistent with other remote sensing observations of TKE dissipation rates which have been often observed to decay from top to bottom (Grimsdell and Angevine (2002),Lothon et al. (2014)).

Before considering the evolution of the spectral characteristics, the turbulence structure evolution during this decay can be investigated with the anisotropy. Here we consider the anisotropy with estimates of the ratio of the horizontal wind variance to the vertical wind variance (Fig. 9b). Before 1630 UTC, it remains smaller than 1 in the mid-PBL, and it is larger than 1 in the uppest and lowest part, due to 'squashed' turbulence close to the interfaces. The predominance of buoyancy during midday leads to a large contribution of the vertical variance in TKE in midday. The ratio gets larger than 1 only after 1730 UTC in the middle of the PBL, but it increases close to the top as early as 1230 UTC: the change in anisotropy, like the TKE, starts early in the upper PBL, with an increasing transfer from vertical to horizontal components along the decay process in the upper part of the PBL.

5.2 Spectral analysis

5.2.1 Evolution of the slopes of the w spectra

The slope of the simulated and observed spectra are first analyzed because i/ they are key characteristics of the spectra and, ii/ the Kristensen spectrum model assumes the theoretical slope for $kS(k)$ value of 1 and -2/3 for low and high wavenumber range, respectively.

Concerning the low wavenumber range, the slopes of the simulated and near-surface observed spectra remain approximately constant during the whole day and close to the theoretical value of one (Fig. 10a). The spectra slopes of airborne measurements are steeper than in the theory and vary from 1.5 to 2.5. This results illustrates the weak statistical representativity of large scales along aircraft flight leading to scattered estimates of the spectra slope in this wavenumber range.

Concerning the slopes in the inertial subrange, both simulated and aircraft data reveal steeper slopes than the theoretical value of $-2/3$, even during the fully convective

period (Fig. 10b). The reason for these steeper slopes has not been fully investigated but anisotropy smaller than 1 (Fig. 9b) or the presence of coherent structures could be involved. Steeper slopes of the inertial subrange were previously observed in different contexts of PBL and with various types of observations with vertically pointing groundbased lidar by Lothon et al. (2009), or with airborne high frequency in situ measurements by Lothon et al. (2007) and would deserve further understanding. At the end of the afternoon, the slopes decrease on both LES and aircraft data with a good consistency. This decrease appears to behave differently according to height in two ways: 1/ it occurs earlier at the top of the PBL (around 1600 UTC), than in the lower layers (after 1745 UTC at 0.15 z_i), 2/ the lower in the PBL, the smaller the increase. These delayed and smaller changes with decreasing altitude seem to be in continuity with what is observed close to surface where the slope follows the theoretical $-2/3$ value during the whole day.

5.2.2 *Characteristic lengthscales*

The integral scale is one of the two spectral characteristics determined from the fit with the Kristensen and Lenschow (1989) analytical spectrum model.

We verified that these integral scale estimates (l_w) were similar to estimates of integral scales (L_w) based on the autocorrelation function (equation 5) which is more generally used. The two methods were found consistent together and gave similar temporal evolution of integral scale. Hereafter, only l_w is considered.

The temporal evolution of l_w obtained with the simulation at different heights, aircraft and surface data are presented in Fig. 11. At midday, the lengthscales verify what is found in litterature, with a value around 200 m in the middle of the mixed layer (Dosio et al., 2005), and smaller lengthscales at the top and at the bottom of the mixed layer because of 'squashed' eddies near wall conditions. l_w remains approximately constant until 1700 UTC, and then increases above 0.15 z_i for both LES and aircraft data. The higher the considered level, the sharper the l_w increase.

Close to surface, l_w is constant until 1700 UTC, with a value of 10 m, and then decreases to 5 m. As expected, the 60 m mast data provides longer l_w than at the surface but very scattered (between 30 and 80 m) preventing an estimate of l_w tendency with time at that height. Note that LES cannot be compared to observations close to surface, due to the observed scales that are smaller or of the order of the horizontal resolution.

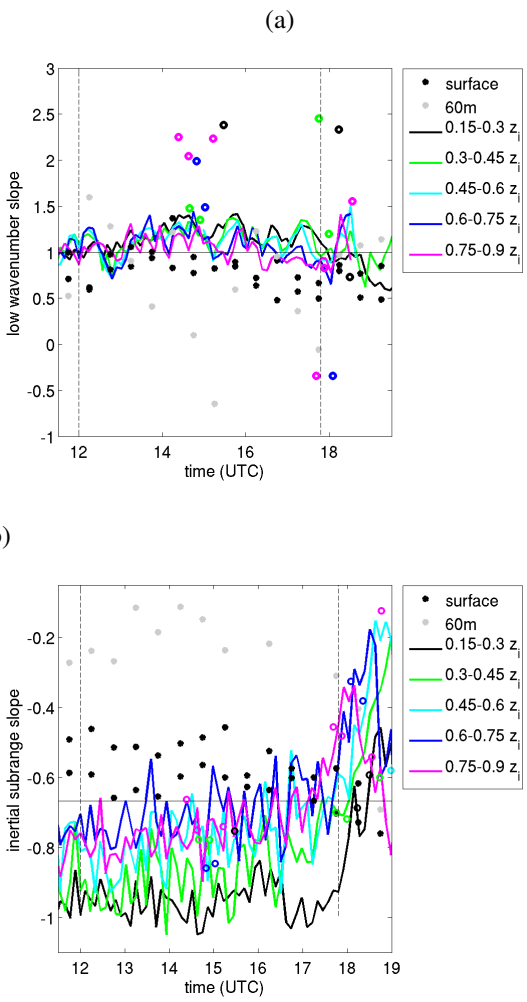

Figure 10: temporal evolution of the slopes in (a) the low wavenumber range and (b) the inertial subrange of the w spectra with les (continuous lines), aircraft and surface measurements (open and filled circles) at different heights (colors).

5.2.3 *Shape of the spectra*

The shape of the spectra is depicted by the μ sharpness parameter (equation 2). Figure 12 shows the temporal evolution of μ that gives the best fit of the spectra for simulation, aircraft and surface data. Above 0.15 z_i, μ is around 2 and remains constant until 1600 UTC, aircraft and simulated data giving similar results. Those results are similar to those found by Lothon et al. (2009) with groundbased lidar, who also observed sharper spectra than Kaimal spectra in the middle of the PBL. After 1600 UTC, μ decreases, meaning that the turbulence spectra flatten during the LAT associated to a broadening of the containing energy wavenumber range above 0.15 z_i. In the contrary, close to surface and at 60 m height, $\mu \approx 0.5$

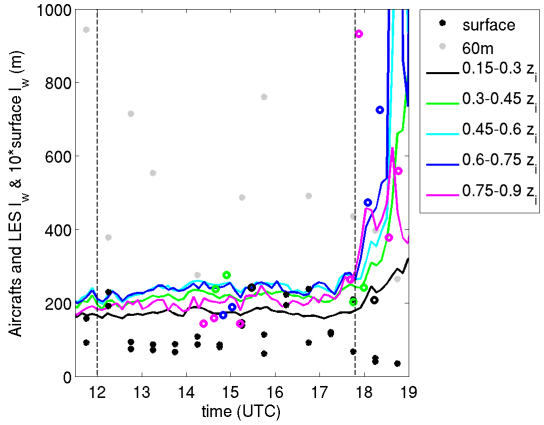

Figure 11: temporal evolution of l_w calculated from the kristensen analytical model with les (continuous lines) and aircraft (open circles) and surface (closed circles) data at different heights (different colors).

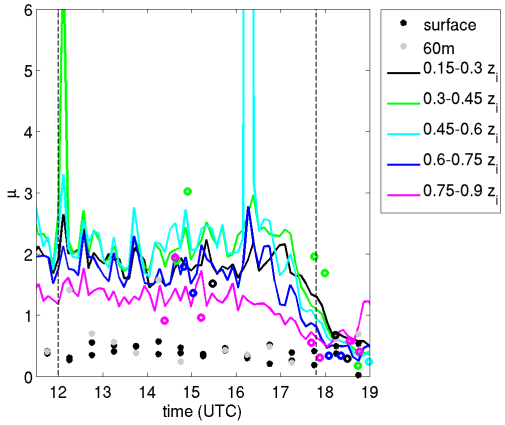

Figure 12: temporal evolution of the parameter μ, obtained from the kristensen analytical model, with les (continous lines), aircraft (crosses) and surface (black stars) data.

throughout the day, which corresponds to the spectrum model from Kaimal et al. (1972) and means that the energy wavenumber range remains large during the LAT. In the Kristensen analytical model, μ, l_w and Λ_w are linked by equation 4 which gives higher ratio Λ_w/l_w for higher μ (Lenschow and Stankov, 1986). Consequently, the decrease of μ associated to an increase of l_w during the LAT implies that Λ_w is drifted toward the larger eddies (as noticed in Fig. 8) but slower than l_w is.

5.3 Timing of the changes

The previous results illustrate the changes of turbulence characteristics throughout the afternoon according to height. The times when these characteristics start to change are now quantified using the simulation data above 0.15 z_i and the measurements at 60 m height and near surface at moor and corn sites. The time of change for the parameter x is noted t_x here after (Fig. 13). For μ, l_w and the slope, the time of significant change is defined when these spectra parameters exceed their mean value plus (for t_{l_w} and t_{slope}) or minus (for t_μ) three times their standard deviation, both calculated between noon and 1400 UTC. Because of the diurnal cycle of the TKE and the horizontal and vertical wind variances, the previous method could not be applied to determine the time change of these parameters. t_{TKE}, $t_{<w'^2>}$ and $t_{<u'^2>^2+<v'^2>}$ were quantified by determining the time when the slope of the decaying parameter becomes larger than an arbitrary threshold of -0.02 $m\,s^{-1}$.

As already noticed in section 5.1, the TKE clearly decreases at the top of the boundary layer height first, and early: half an hour after the start of the afternoon transition (Fig. 13). This decrease propagates from z_i towards the lower layers (0.15 z_i) within the following hour. The TKE decrease is exclusively driven by the vertical velocity component variance, which decreases at the top of the PBL one and half hour before the maximum surface buoyancy flux. The early decrease of the wind vertical variance is counter balanced in TKE by the late change of the horizontal wind variance. This implies an increase of anisotropy from wind component variances point of view in the early stage of surface flux decrease.

The change on other spectrum parameters is observed much later, during the last two hours before the surface buoyancy flux reaches zero. The three vertical profiles of t_{l_w}, t_{slope} and t_μ, indicate a flattening and a shift of the spectra toward the small wavenumbers, with an increase of the inertial subrange slope, appearing first at the top of the boundary layer and rapidly propagating toward the lower layers.

Near the surface and at 60 m height, a very weak evolution of the spectra is observed. The spectra keep the same sharpness, similar to Kaimal spectra, with a constant slope of $kS(k)$ of $-2/3$ in the inertial subrange, a constant value of μ of 0.5 throughout the afternoon and a very slightly decreasing l_w. These results are consistent with spectra behavior above 0.15 z_i. Indeed, μ decreases from around 2 in convective conditions to 0.5 at the end of the afternoon transition in the whole upper layer and the l_w increase in the upper layers is less and less pronounced with decreasing height.

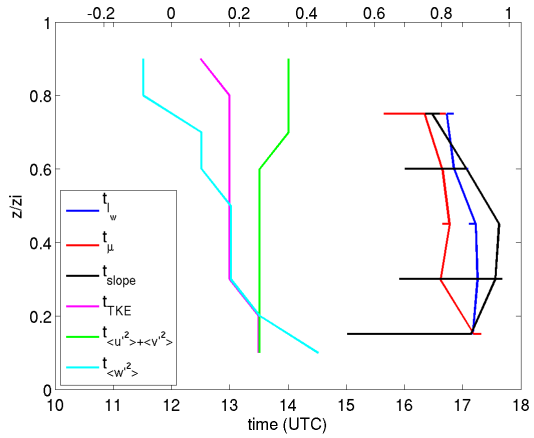

Figure 13: vertical profiles of the timings of changes observed in the evolution of the tke, the vertical and horizontal variances, l_v, μ and the inertial subrange slope of w spectra.

5.4 Discussion

The above analysis of the evolution of the turbulence structure during the afternoon transition suggests us to separate this period in two stages.

In the first part of the afternoon, from when the surface buoyancy flux starts to decrease until about two hours before sunset, (i) the TKE decreases within the whole PBL depth, with a one-hour subtil delay between the upper part (earlier decay) and the lower part of the PBL (postponed decay), (ii) the vertical profile of anisotropy does not change much within the PBL, except close to the top. (iii) the spectra keep the characteristics of fully-developped CBL, with the same integral scales and same sharpness parameter.

In the second part of the afternoon, from two hours before sunset until when the buoyancy flux is zero at surface, (i) the TKE decreases more rapidly than previously within the whole PBL depth, (ii) the anisotropy increases abruptly within the PBL, starting first close to the top, (iii) the shape of the spectra evolves, with a decrease of the sharpness parameter, a flattening of the inertial subrange slope, an increase of the integral lengthscales in the mid and upper PBL. The higher within the PBL, the stronger the increase of the integral scales, with very slight changes of the spectra shape observed close to the surface.

Our understanding of those two different stages of the afternoon transition is that during the first stage, the buoyancy flux remains large and its decay is slow enough, to give time to the CBL to adjust to the change and remain in quasi-steady balance. In other words, the convective time scale t_* is small enough ($\sim$ 9 min) relative to τ_f ($\sim$ 5.8 h), to allow this quasi-steady state. The spectral characteristics remain similar to what they are at maximum surface buoyancy flux. Buoyancy remains of dominant influence during this stage, which leaves predominancy to the vertical velocity variance and coherent structures which keep the spectral peak sharp. This might also be at the origin of the steep inertial subrange slope. It should be noted that an inertial subrange slope should theoretically be expected from fully developped turbulence. Those results (on the vertical wind only) seem to infer that the turbulence production as theoretically expected is observed only near the ground.

To the contrary, during the second stage, the t_* increases (about 20 min at 1700 UTC) and the buoyancy flux gets too small for the PBL to maintain the vertical coherency of the turbulence structure from surface up to the top of the PBL. The classical features of convective conditions may not be relevant anymore during this stage, as the quasi-steady balance is lost (Lothon et al., 2014). The role of buoyancy decreases a lot during this period, relative to the role of entrainment. Although entrainment flux is decaying as well at the top, it is influencing a deeper and deeper layer from top down to 0.4 z_i. Consistently with Lohou et al. (2010), this could explain the increase of vertical velocity integral scales. The increase of integral scales that we find in the upper PBL during this second stage is consistent with Sorbjan (1997) and Grant (1997), but differ from the results of Pino et al. (2006). This could be the result of the progressive cease of the surface flux in the former studies, versus the sudden shut-off in the latter. Concerning now the surface layer, the decrease of the integral scales in that part of the PBL is consistent with the observations made by Grant (1997) and with the results of Kaimal et al. (1972).

The flatening observed in the inertial subrange during the second stage is difficult to explain, because one could expect a faster drop of this subrange with increasing wavenumber (that is steeper slope in inertial subrange) when the flow moves from turbulent to laminar, also having in mind that the smaller scales will dissipate faster than the larger scales. But several hypotheses could be made to explain the observed flatening of the spectra in inertial subrange: (i) the increase of anisotropy might be associated with such change of the cascade, (ii) the spectrum peak could be spreading over such a large domain that the inertial subrange would be pushed at much smaller scales, although the high resolution of the aircraft measurements (2 to 4 m) allow us to reject this hypothesis, (iii) the ceasing of the interaction of the surface layer with the outer layer could appear as an increase of energy at smaller scale and result in this decrease of the slope in inertial subrange (Hunt and Morrison, 2000), (iv) if the turbulence is now freely decaying, without influence of

coherent structures and vertical velocity dominancy, the cascade could become more efficient, resulting in flatening slope (Moeng and Wyngaard, 1988). In any case, it seems that with the turbulence being no longer fully developped, the criteria for locally isotropic turbulence are no longer met. It it interesting to note that Wroblewski et al. (2010) have found greater anisotropy associated with weaker turbulence, based on aircraft measurements in the upper troposphere and lower stratosphere. And Mestayer (1982) have found that local isotropy was fulfilled only at dissipative length scales in a wind tunnel.

The progressive shut-off of the surface heat fluxes is shown to be an important condition to simulate the afternoon transition processes. Nieuwstadt and Brost (1986) and Pino et al. (2006) who analyzed simulations with a sudden shut-off of the buoyancy flux pointed out what they called a demixing process whose one of the effects was a strong negative buoyancy flux within the whole PBL. The impact of the entrainment in that cases might be over-estimated. In our case, and similarly to Sorbjan (1997), when a shift of the major role is progressively simulated through the afternoon from surface buoyancy to entrainment at the top, the demixing process intensity is strongly reduced and limited to the half-upper part of the PBL.

Nieuwstadt and Brost (1986) and Pino et al. (2006) also found that entrainment is important during the decay, and delays the decay. In our simulation, the dynamical production is very small at the top, still smaller close to surface. So the entrainment, although present, does not seem to delay the decay. Shaw and Barnard (2002) studied the decay with DNS, based on a realistic surface flux decay. Similarly to our study, they observe that the turbulence is maintained at surface relative to upper layers, which they explain with shear at surface.

6. Conclusions

This study leans on the use of analytical spectra to depict and quantify the changes of the spectra shape of the vertical component of the wind throughout the afternoon transition and according to height. Aircraft and surface station measurements of the BLLAST experiment dataset are used to study the turbulence spectra evolution on the 20th of July 2011. A Large Eddy Simulation constrained by observed conditions during BLLAST experiment but further idealized allows a continuous spectra analysis in time and height.

The simulated data, even with an idealized simulation, are in good coherence with the airborne and surface observations. The results show that the model simulates very well the turbulence structure along the afternoon with a resolution and a domain size allowing a good fit of the simulated spectra with the analytical model above 0.15 z_i.

Two main conclusions can be drawn from this study, giving essential highlights on the turbulence evolution from the temporal and vertical point of views.

This study shows for the first time the different steps of the afternoon transition, defined in previous studies as the period starting at the maximum surface bouyancy flux and ending when the buoyancy flux reaches zero. The first step (from 0 to 0.75 τ_f) is characterized by a low-rate decrease of the level of energy but the turbulence characteristics remain the same than during fully convective conditions: same turbulence length scale, same characteristics of the cascade from large to small eddies. During the second step (from 0.75 to 1 τ_f), the TKE decay rate increases and the turbulence characteristics evolve sharply implying very different eddy size and energy transfer. This period is suggested to be called the Late Afternoon Transition (LAT) in Lothon et al. (2014).

The second important point concerns the vertical turbulence evolution. The changes observed either on TKE decay (during the first step) or on w spectra shape (during the second step of the afternoon transition) are first observed at the top of the boundary layer. Furthermore, the higher within the PBL the stronger the spectra shape changes. These results show that, in our study, the top of the boundary layer is first affected by the changes which progressively go down toward surface.

One can wonder wether these results could be impacted by the initial conditions (such as wind strength and wind shear). The use of all the airborne measurements acquired during the BLLAST experiment shows the general trend of an increasing integral scale during the LAT (not shown). However it would be useful to complete this study with some other LES studies either using some other BLLAST IOPs or with some sensitivity tests.

At last, whilst the Large Eddy Simulation is a valuable tool to complete the observations, the use of the DNS would help a lot in the understanding of the spectra shape changes.

Acknowledgements

The BLLAST field experiment was made possible thanks to the contribution of several institutions and supports : INSU-CNRS (Institut National des Sciences de l'Univers, Centre national de la Recherche Scientifique, LEFE-IMAGO program), Mto-France, Observatoire Midi-Pyrnes (University of Toulouse), EUFAR (EUropean Facility for Airborne Research) BLLATE-1&2, COST ES0802 (European Cooperation in the field of Scientific and Technical) and the Spanish MINECO projects CGL200908609, CGL201237416C0403, and CGL2011-13477-E. The field experiment would not have occurred without the contribution of all participating European and American research groups, which all have contributed in a significant

amount. The Piper Aztec research airplane is operated by SAFIRE, which is a unit supported by INSU-CNRS, Mto-France and the French Spatial Agency (CNES). BLLAST field experiment was hosted by the instrumented site of Centre de Recherches Atmosphriques, Lannemezan, France (Observatoire Midi-Pyrnes, Laboratoire dArologie). Its 60 m tower is partly supported by the POCTEFA/FLUXPYR European program. BLLAST data are managed by SEDOO, from Observatoire Midi-Pyrnes. Since 2013, the French ANR supports BLLAST analysis. See http://bllast.sedoo.fr for all contributions. We particularly thank Eric Pardyjak, Oscar Hartogensis, Dominique Legain, and Frédérique Saïd, for providing the surface measurements used in this study.

REFERENCES

Blay-Carreras, E., D. Pino, A. Van de Boer, O. De Coster, C. Darbieu, O. Hartogensis, F. Lohou, M. Lothon, H. Pietersen, and J. Vilà-Guerau de Arellano, 2014: Role of the residual layer and largescale subsidence on the development and evolution of the convective boundary layer, *Atmos. Chem. Phys.*, **13**, 31527–31662.

Cole, G. and H. J. S. Fernando, 1998: Some aspects of the decay of convective turbulence, *Fluid Dynamics Research*, **23**, 161–176.

Davidson, P., 2004: *Turbulence: An introduction for Scientists and Engineers*.

Deardorff, J. W., 1970: Convective velocity and temperature scales for the unstable planetary boundary layer and for Rayleigh convection, *Journal of the Atmospheric Sciences*, **27**, 1211–1215.

Dosio, A., J. Vilà-Guerau De Arellano, and A. A. M. Holtslag, 2005: Relating Eulerian and Lagrangian Statistics for the Turbulent Dispersion in the Atmospheric Convective Boundary Layer, *Journal of the Atmospheric Sciences*, **62**, 1175–1191.

Fitzjarrald, D. R., J. M. Freedman, M. J. Czikowsky, R. K. Sakai, and O. L. L. Moraes, 2004: Momentum and scalar transport during the decay of CBL turbulence, *16th AMS Symposium on boundary layers and turbulence*, **, 1**.

Gioli, B., M. Miglietta, F. P. Vaccari, A. Zaldei, and B. De Martino, 2009: The Sky Arrow ERA, an innovative airborne platform to monitor mass, momentum and energy exchange of ecosystems, *Annales Geophysicae*, **49**, 109–116.

Goulart, A., G. Degrazia, U. Rizza, and D. Anfossi, 2003: A theoretical model for the study of convective turbulence decay and comparison with large-eddy simulation data, *Boundary-Layer Meteorology*, **107**, 143–155.

Grant, A. L. M., 1997: An observational study of the evening transition boundary-layer, *Quarterly Journal of the Royal Meteorological Society*, **123, 1997**, 657–677.

Grimsdell, A. W. and W. M. Angevine, 2002: Observations of the afternoon transition of the convective boundary layer, *Journal of Applied Meteorology*, **41**, 3–11.

Heo, B., S. Jacoby-Koaly, K. Kim, B. Campistron, B. Bénech, and E. Jung, 2003: Use of the Doppler spectral width to improve the estimation of the convective boundary layer height from UHF wind profiler observations, *Journal of Atmospheric and Oceanic Technology*, **20, 3**, 408–424.

Hojstrup, J., 1982: Velocity spectra in the unstable planetary boundary layer, *Journal of the Atmospheric Sciences*, **39**, 2239–2248.

Hunt, J. C. and J. F. Morrison, 2000: Eddy structure in turbulent boundary layers, *European Journal of Mechanics - B/Fluids*, **19**, 673–694.

Jacoby-Koaly, S., B. Campistron, S. Bernard, B. Bénech, F. Ardhuin-Girard, J. Dessens, E. Dupont, and B. Carissimo, 2002: Turbulent dissipation rate in the boundary layer via uhf wind profiler doppler spectral width measurements, *Boundary-Layer Meteorology*, **103**, 361–389.

Kaimal, J., J. Wyngaard, and O. Coté, 1972: Spectral characteristics of surface layer turbulence, *Quarterly Journal of the Royal Meteorological Society*, **98**, 653–689.

Kaimal, J., J. Wyngaard, D. Haugen, O. Coté, and Y. Izumi, 1976: Turbulence structure in the convective boundary layer, *Journal of the Atmospheric Sciences*, **33**, 2152–2169.

Kàrmàn, T., 1948: Progress in the statistical theory of turbulence, *Proc Nat Akad Sci*, **34**, 530–539.

Kristensen, L. and D. H. Lenschow, 1989: The spectral velocity tensor for homogeneous boundary-layer turbulence, *Boundary-Layer Meteorology*, **47**, 149–193.

Legain, D., O. Bousquet, T. Douffet, D. Tzanos, E. Moulin, J. Barrie, and J.-B. Renard, 2013: High frequency boundary layer profiling with reusable radiosondes, *Atmos. Meas. Tech. Discuss.*, **6**, 3339–3365.

Lenschow, D. H. and B. B. Stankov, 1986: Length scales in the convective boundary layer, *Journal of the Atmospheric Sciences*, **43**, 1198–1209.

Lohou, F., F. Saïd, M. Lothon, P. Durand, and D. Serça, 2010: Impact of Boundary-Layer Processes on Near-Surface Turbulence Within the West African Monsoon, *Boundary-Layer Meteorology*, **136, 1**, 1–23.

Lothon, M., D. H. Lenschow, and S. D. Mayor, 2009: Doppler Lidar Measurements of Vertical Velocity Spectra in the Convective Planetary Boundary Layer, *Boundary-Layer Meteorology*, **132, 2**, 205–226.

Lothon, M., D. H. Lenschow, and A. Schanot, 2007: Status-reminder report on C-130 air-motion measurements. Test of DYCOMS-II new datasets, *Internal report, NCAR-RAF*.

Lothon, M., F. Lohou, D. Pino, E. Pardyjak, J. Reuder, F. Couvreux, P. Durand, I. Faloona, O. Hartogensis, D. Legain, W. M. Angevine, P. Augustin, E. Bargain, E. Bazile, E. Blay-Carreras, J. L. Boichard, A. Bourdon, A. Butet, O. D. Coster, J. Cuxart, A. Dabas, C. Darbieu, K. Deboudt, S. Derrien, P. Flament, M. Fourmentin, A. Garai, F. Gibert, B. Gioli, A. Graf, J. Groebner, F. Guichard, M. Jonassen, E. Magliulo, S. Martin, D. Martinez, L. Mastrorillo, A. F. Moene, F. Molinos, E. Moulin, H. Pietersen, B. Piguet, E. Pique, Y. Seity, G. J. Steeneveld, P. Toscano, D. Tzanos, S. Wacker, N. Wildmann, and A. Zaldei, 2014: The BLLAST field experiment: Boundary- Layer Late Afternoon and Sunset Turbulence, *Atmos. Chem. Phys. Discuss*, **4, 14**, 10789–10852.

Mestayer, P., 1982: Local isotropy and anisotropy in a high-reynoldsnumber turbulent boundary-layer, *Journal of Fluid Mechanics*, **125**, 475–503.

Moeng, C. H., 1984: A large-eddy-simulation model for the study of planetary boundary-layer turbulence, *Journal of the Atmospheric Sciences*, **41**, 2052–2062.

Moeng, C. H. and J. Wyngaard, 1988: Spectral-analysis of large-eddy simulations of the convective boundary-layer, *Journal of Atmospheric Sciences*, **45**, 3573–3587.

Monin, A. S. and A. M. Yaglom, 1975: *Statistical fluid mechanics*, volume 2, john l. lu edition.

Nadeau, D. F., E. Pardyjak, C. W. Higgins, H. J. S. Fernando, and M. B. Parlange, 2011: A Simple Model for the Afternoon and Early Evening Decay of Convective Turbulence Over Different Land Surfaces, *Boundary-Layer Meteorology*, **141, 2**, 301–324.

Nieuwstadt, F. T. M. and R. A. Brost, 1986: The decay of convective turbulence, *Journal of the Atmospheric Sciences*, **43**, 532–546.

Patton, E. G., P. P. Sullivan, Moeng, and C. H., 2005: The Influence of Idealized Heterogeneity on Wet and Dry Planetary Boundary Layers Coupled to the Land Surface, *Journal of the Atmospheric Sciences*, **62**, 2078–2097.

Pino, D., H. J. J. Jonker, J. Vilà-Guerau De Arellano, and A. Dosio, 2006: Role of Shear and the Inversion Strength During Sunset Turbulence Over Land: Characteristic Length Scales, *Boundary-Layer Meteorology*, **121, 3**, 537–556.

Rizza, U., M. Miglietta, G. Degrazia, O. Acevedo, and E. Marques Filho, 2013: Sunset decay of the convective turbulence with Large-Eddy Simulation under realistic conditions, *Physica A: Statistical Mechanics and its Applications*, **392, 19**, 4481–4490.

Saïd, F., U. Corsmeier, N. Kalthoff, C. Kottmeier, M. Lothon, a. Wieser, T. Hofherr, and P. Perros, 2005: ESCOMPTE experiment: intercomparison of four aircraft dynamical, thermodynamical, radiation and chemical measurements, *Atmospheric Research*, **74, 1-4**, 217–252.

Shaw, W. and J. Barnard, 2002: Scales of turbulence decay from observations and direct numerical simulation, *Proceedings of the 15th Symposium on Boundary Layers and Turbulence*.

Sorbjan, Z., 1997: Decay of convective turbulence revisited, *Boundary-Layer Meteorology*, **82**, 501–515.

Sullivan, P. P. and E. G. Patton, 2011: The Effect of Mesh Resolution on Convective Boundary Layer Statistics and Structures Generated by Large-Eddy Simulation, *Journal of the Atmospheric Sciences*, **68, 10**, 2395–2415.

Wroblewski, D., O. Cote, J. Hacker, and R. Dobosy, 2010: Velocity and Temperature Structure Functions in the Upper Troposphere and Lower Stratosphere from High-Resolution Aircraft Measurements, *Journal of the Atmospheric Sciences*, **67**, 1157–1170.